Available online at www.sciencedirect.com
SCIENCE DIRECT
Journal of volcanology and geothermal research
ELSEVIER
Journal of Volcanology and Geothermal Research 154 (2006) 181–200
www.elsevier.com/locate/jvolgeores

Apparent migration of tremor source synchronized with the change in the tremor amplitude observed at Aso volcano, Japan

Noriaki Takagi [a,*], Satoshi Kaneshima [b], Hitoshi Kawakatsu [c], Mare Yamamoto [d], Yasuaki Sudo [e], Takahiro Ohkura [e], Shin Yoshikawa [e], Takehiko Mori [f]

[a] *Tokyo Institute of Technology, 1-12-1 Ohokayama Meguroku Tokyo, Japan*
[b] *University of Kyushu, 6-10-1 Hakozaki Higashi-ku Fukuoka, Japan*
[c] *Earthquake Research Institute, University of Tokyo, 1-1-1 Yayoi Bunkyo-ku Tokyo, Japan*
[d] *Tohoku University, 6-3 Aoba Aramaki Aoba-ku Sendai-shi, Japan*
[e] *Aso Volcanological Laboratory, Kyoto University, 5280 Kawayo tyouyou-mura Aso-gun Kumamoto-ken, Japan*
[f] *Geological Survey of Japan, 1-1-1 Higashi Tsukuba-shi Ibaraki-ken, Japan*

Received 21 December 2004; received in revised form 15 December 2005; accepted 1 February 2006
Available online 20 March 2006

Abstract

At Aso volcano, Kyushu, Japan, several different types of volcanic tremor have been observed for many years. One of them is the continuous tremor, the ground vibration which has dominant frequency between 3 and 10 Hz and has approximately constant amplitudes without any clear beginning and ending. We observed the continuous tremor at Aso using short period seismometer arrays for 3 days in 1999. We locate the source of the continuous tremor by seismic array data processing. We use the semblance coefficients in order to estimate the arrival azimuth and apparent slowness by grid search. The epicenters of the continuous tremor are located around the currently active crater, and the source depths are likely to be shallower than 600 m. We find that the estimated epicenter clearly migrates synchronized with the change in the tremor amplitude. The migration often occurs periodically with a period of about 80 s, but aperiodic occurrence of the migration is also often seen. In both cases, the epicenter is located southeastward (northwestward) when the amplitude is larger (smaller). We propose that there are two or more independent tremor sources with fixed locations, and that their amplitudes modulate either aperiodically or periodically with periods nearly 80 s. The tremor signals from those sources are mixed at the arrays, and the estimated epicenter parameters vary according to which signal dominates the seismograms. The simplest model is that there are two point sources, one at west and the other at south of the crater (we call the two sources as "NW source" and "SE source", respectively), and the amplitude of the SE source changes with time. Consequently, the SE source dominates the seismogram when the observed amplitude is larger, whereas the NW source dominates when the amplitude is smaller. We generate synthetic seismograms, and apply the location technique to them to verify the validity of the two point source model and to search the locations of two sources which can explain the observed synchronization between the amplitude and the apparent epicenter location. We find that the distance between the two sources needs to be more than 400 m to agree with the observation. We also analyze the seismic array data observed in 2001, and infer that the NW source in 1999 may be identical to the tremor source of the 2001 data.

Keywords: volcanic tremor; tremor; array; semblance; amplitude modulation

* Corresponding author. Fax: +81 3 5734 3538.
E-mail address: ntakagi@geo.titech.ac.jp (N. Takagi).

0377-0273/$ - see front matter © 2006 Elsevier B.V. All rights reserved.
doi:10.1016/j.jvolgeores.2006.02.001

1. Introduction

1.1. Volcanic tremor and locating its sources

Excitation of volcanic tremor is one of the most important seismic phenomena at active volcanoes. Observations of volcanic tremor are practically important because they can be utilized in eruption warning and volcanic hazard mitigation. From a purely scientific point of view, on the other hand, volcanic tremors are often conceived to represent fluid motion in the edifice of volcanoes. For that purpose, volcanic tremors have been observed at many active volcanoes around the world. Their characteristics vary from volcano to volcano or change with time even for one volcano. Chouet (1996) classified seismic activities at volcanoes into VT and LP seismicity. A VT (volcano-tectonic earthquake) is a shear faulting in solid rock, which is the same process as a tectonic earthquake. On the other hand, LP seismicity is considered to originate in pressure fluctuations of the fluid surrounded by solid rocks, and includes LP events and tremor. LP events have a typical period of 0.2–2 s with durations of few tens of seconds. On the other hand a tremor is a sustained oscillation whose duration ranges from minutes to days, or even longer on some occasions. LP events and tremors have similar spectra, slownesses, and source locations at many volcanoes such as Kilauea (Almendros et al., 2001), and Montserrat (Neuberg et al., 2000).

The source location of a volcanic tremor is one of the most important pieces of information. But it is usually difficult to accurately locate a tremor source because P and S waves cannot be distinguished clearly on the tremor seismograms, and wave forms often significantly vary from receiver to receiver due to large site and path effects for volcano edifices. These difficulties could be overcome to some extent by deploying dense seismic arrays. Recent developments in seismometry have enabled us to discriminate difference in the phase of seismic waves from receiver to receiver, which can be converted to the time lag. We therefore can estimate apparent slowness (which is inverse of apparent velocity) and back azimuth of tremor signals with reasonable accuracy by using seismic array technique. There are several different kinds of methods for determining apparent velocities of seismic wave fields for locating the wave source. The frequency domain methods include the f–k spectrum method (Lacoss et al., 1969), the cross spectrum method (Ito, 1985), and the MUSIC technique (Goldstein and Archuleta, 1987; Goldstein and Chouet, 1994; Chouet et al., 1997; Almendros et al., 2001; Saccorotti et al., 2004). On the other hand, the time domain methods for locating sources of volcano-seismic signals utilize, for instance, the cross correlation function (Almendros et al., 1999; Ibanez et al., 2000), or the semblance coefficient (Neidel and Taner, 1971; Kawakatsu et al., 2000). In this study we use semblance-based techniques in order to locate the source of the continuous tremor at Aso volcano, in Kyushu, Japan.

1.2. Volcanic activity at the Aso volcano

The Aso volcano is one of the most prominent active volcanoes in Japan (Fig. 1). There are 7 craters at the Naka-dake summit, the first of which currently emits volcanic gases (star in Fig. 1). We call this crater as the main crater. The last magmatic eruption occurred from 1989 to 1991 at this crater. Except for the gas emission, there was no significant volcanic activity at the surface during the observations in 1999. Although such a quiet stage of volcanic activity has continued for more than 10 years at Aso, volcanic tremors have always been observed. The volcanic tremors at Aso have been historically classified according to their dominant periods by Sassa (1935). By updating his classification, we classify seismic signals of volcanic origin at Aso as follows:

Type a) Long period events with the period of 15 s.
Type b) High frequency (shorter period) tremor with dominant frequency around 3 to 10 Hz, which occurs continuously. We call this type of tremor as “continuous tremor”, or simply as “tremor”.
Type c) An isolated events with dominant frequency around 1 to 2 Hz.

The source of the Type a events is located accurately at depths of 1 to 1.5 km about 400 m south-west of the main crater (Kaneshima et al., 1996; Legrand et al., 2000; Kawakatsu et al., 2000). The kinematic description of the source mechanism of the Type a events is a combination of isotropic expansion/contraction and an inflation/deflation of an inclined tensile crack (Kaneshima et al., 1996; Yamamoto et al., 1999; Legrand et al., 2000). As for the higher frequency signals (Type b or c), Kikuchi (1963) proposed that the tremor of 2–5 Hz consists of surface waves produced by small volcanic earthquakes. Signals of the Type c events continue nearly 20 s and are sometimes preceded by an even higher frequency volcanic signals of 10 Hz (Mori, 2000). Moreover the Type c events occur almost simultaneously with

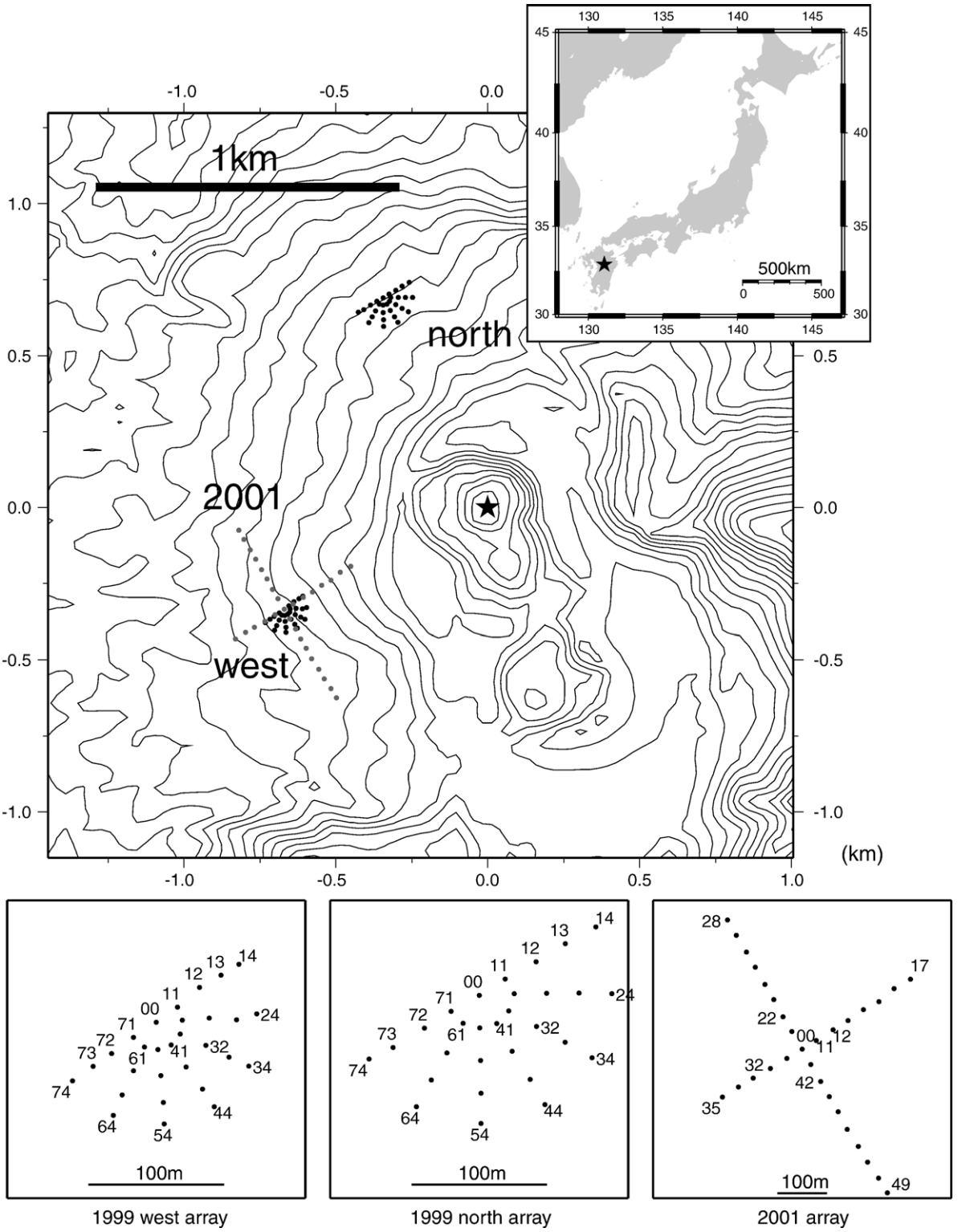

Fig. 1. (Top) Location of Mt. Aso (inset) and a topography map of the Aso volcano. Star marks the center of the Naka-dake main crater. Solid dots show the locations of the sensors of the 1999 arrays (dark) and the 2001 array (light), respectively. Contour interval of the topograph is 15 m. (Bottom) Enlarged maps of the arrays.

the Type a events (e.g., Kaneshima et al., 1996). Mori (2000) investigates some events of Type c and concludes that the sources are located at southeast of the main crater, at a depth of about 600 m. Yamamoto (2004) analyzes the Type c events, and concludes that the source mechanism mainly consists of a radial motion of the sidewall of a nearly vertical cylinder.

Based on the preliminary results from the array analyses of the continuous tremor (Type b) that it has a larger apparent slowness than the Type c events, Takagi (2002) concludes that the source of the Type b tremor is shallower than that of Type c events. Another notable observation of the continuous tremor (Type b) is that during the observation in November 1999, its amplitude modulated either periodically or aperiodically. This is a rather rare phenomenon for the Aso volcano, whose occurrence continued only a few months. In this study we investigate the relationship between the modulation and the source location. The results offer some valuable hints to understand the mechanism of the continuous tremor at the volcano in a quiet stage.

2. Observation

2.1. The 1999 observation

For three days in November, 1999, two seismometer arrays were deployed near the Naka-dake main crater by

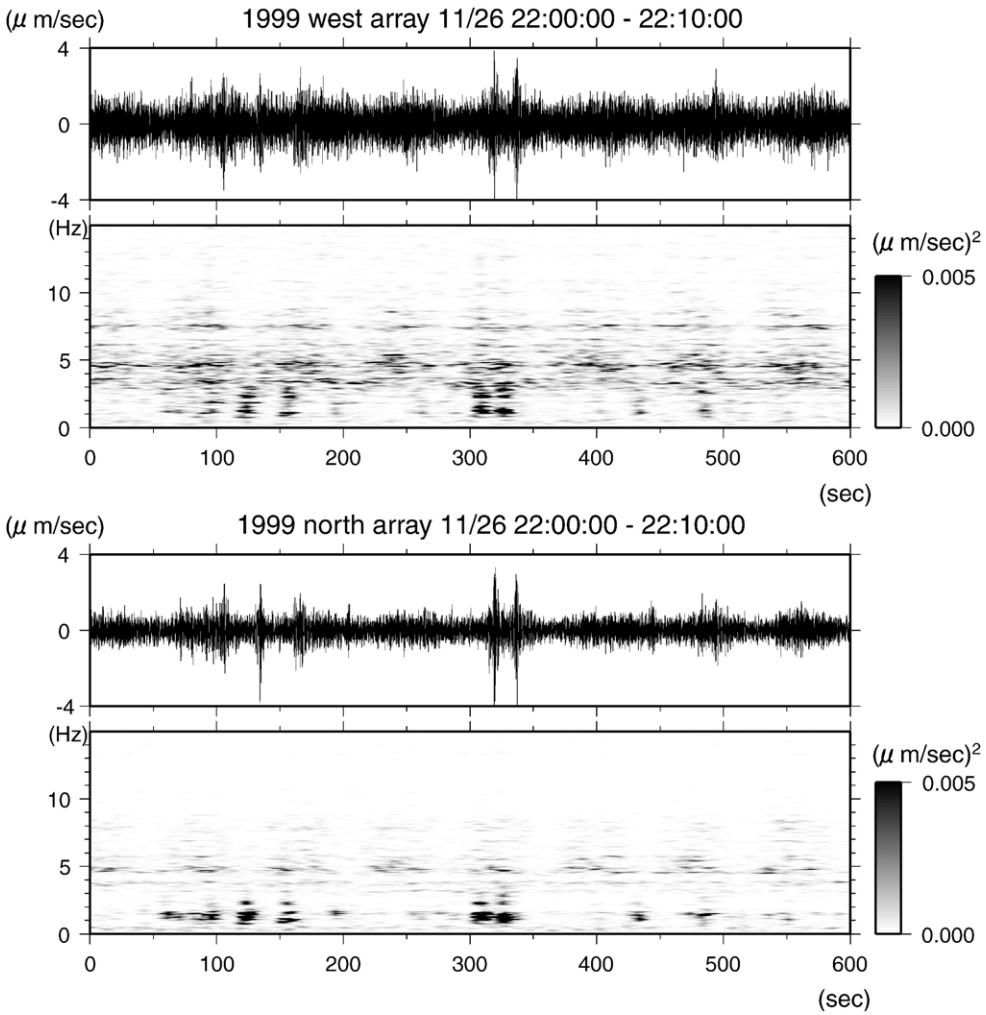

Fig. 2. Examples of the vertical component velocity seismograms observed at the center (sensor 00) of the west array during the 1999 observation and spectrogram. The horizontal axis represents time in seconds. The vertical axis of the spectrogram is frequency from 0 to 15 Hz. The power spectra are shown with gray scale. An amplitude modulation with a period of 80 s can be seen. (Top) An example of seismogram and spectrogram for the vertical component observed during the 1999 observation at the west array for 10 min from 22:00 to 22:10, on Nov. 26, 1999. The sensor is at the array center. (Bottom) Seismogram and spectrogram observed at the sensor 00 of the north array during the same period as the top panel.

a joint team of Tokyo Institute of Technology, University of Tokyo, and University of Kyoto in order to observe volcanic tremors. As shown in Fig. 1, the arrays were installed at west and north of the main crater, nearly 700 m from the center of the crater lake. Hereafter we call these arrays 'the west array' and 'the north array', respectively. Each array consisted of 29 seismographs with a semi-circular form. The aperture lengths of the west and north arrays were 160 and 200 m, respectively. At stations 00, 14, 24, 34, 44, 54, 64, and 74 which were located at the outer rim of the semi-circular arrays, three component velocity seismometers with a free period of 1 s (Lennartz LE-3D) were installed, while at other stations vertical component velocity seismometers with a free period of 0.5 s (Mark Products, L22D) were installed. Seismic signals were digitized with 16 bits and stored in data loggers with a 20 M bytes static memory (LS-8000SH, HAKUSAN). The sampling rate was 0.01 s, and the internal clocks of the data loggers were corrected with GPS signals once every hour giving high enough accuracy of timing. The observations were performed for three nights (33 h). The locations of the stations were determined by the GPS quick static location technique, with high enough accuracy (on the order of 10 cm) of the relative locations of the stations.

2.2. Characteristic features of the data

Figs. 2 and 3 show examples of the spectrograms and seismograms, respectively. During the 1999 observation, many Type c events were recorded. We can see isolated events (Type c) in Fig. 2 at about 100, 120, 150, 310, and 325 s. Most of the isolated events last for 10 to 20 s. The continuous tremor lasts at least for several years, and it is seen throughout the time window in Fig. 2. The dominant frequency band of the continuous tremor (Type b) is from 3 to 10 Hz. The particle motion of the tremor is complicated. At the west array, the motion in the direction transverse to the center of the crater lake (called 'transverse') is dominant. On the other hand, the direction of the dominant motion scatters among the sensors at the north array.

The amplitude of the continuous tremor during the 1999 observation sometimes modulated periodically. Such a periodic amplitude modulation of the continuous

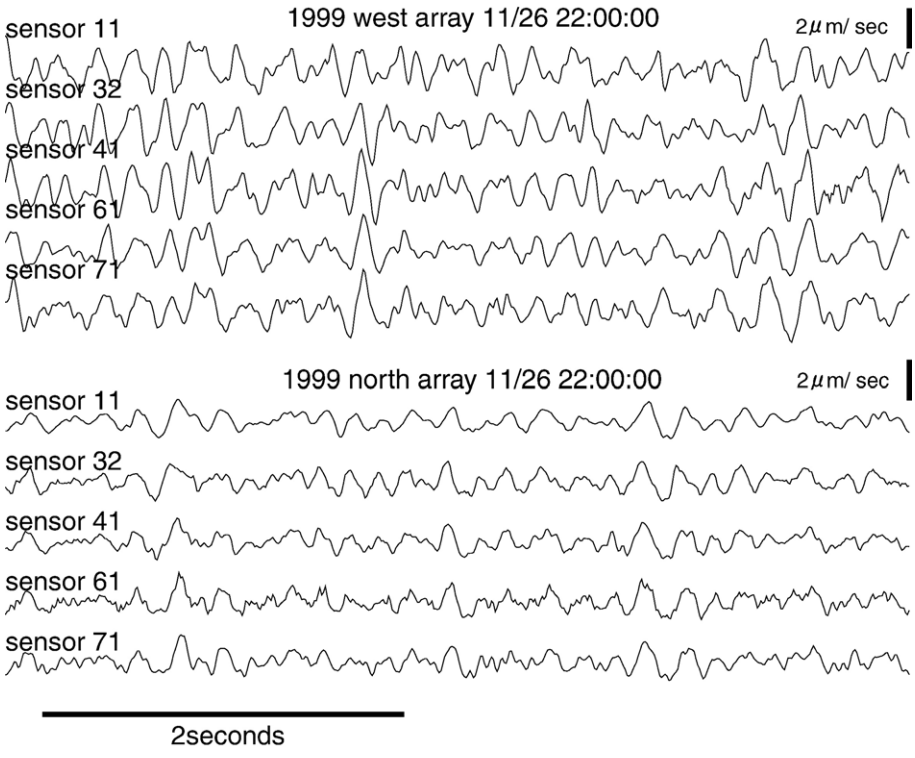

Fig. 3. (Top) The vertical component velocity seismograms observed at selected sensors of the west array during the 1999 observation. The first 5 s of Fig. 2 is shown. See Fig. 1 for the sensor locations. The seismograms are dominated by the continuous tremor for this time window. Coherent arrivals of signals are seen across the array. (Bottom) Examples for the vertical component seismograms observed at the north array during the 1999 observation for the same time window as above.

tremor seems a rather rare phenomenon at Aso, although it lasted for a few months in late 1999. During the 1999 observation, the period of the modulations was about 80 s (Fig. 2). To quantify this phenomenon we calculate moving averages of the absolute value of the amplitude at sensor 00 of the west array over a time window of 10 s, obtaining a time series of smoothed absolute values with a time interval of 1 s. We then compute auto-correlation coefficients of the smoothed absolute values for each hour of the observation. The result is shown in Fig. 4. The periodic amplitude modulation appears intermittently during three days of the 1999 observation. Even when such periodic amplitude modulating is not seen, the tremor amplitudes change with time. We call these 'aperiodic amplitude modulations'.

3. Method of searching tremor source parameters

3.1. Grid search method with semblance coefficient

In this study, we estimate two parameters, θ and s, which represent the azimuth of the epicenter from the array and the apparent slowness of seismic waves, respectively. The seismic signals are regarded as plane waves propagating horizontally so that the hypocentral depth is not determined. The velocity structure is assumed to be homogeneous. We also take an assumption that the sensors are on the same horizontal plane although the maximum difference in the height among the sensors amounts to 20 m for the west array of the 1999 experiment. We use the semblance coefficient (Neidel and Taner, 1971), S, in our seismic array analyses. The time series of signal at the n-th sensor is indicated as $u_n(t_m)$ where t_m is the m-th time step, while the time lag of the wave for the n-th sensor is written as τ_n:

$$\tau_n = -s(X_n \cos\theta + Y_n \sin\theta) \tag{1}$$

where X_n and Y_n are the cartesian coordinates of the n-th sensor relative to the center of the array, and θ is the back azimuth of the incident wave measured counter-clockwise from the east. The x and y axes correspond to east and north, respectively. The total number of sensor is N (=29). The number of the data points contained in the time window and the sampling interval are M and Δ, respectively. Therefore t_m is written as $t_m = m\Delta$. The time window to be used for the n-th sensor starts from $t_{m_0} = m_0\Delta + \tau_n$, and ends at $t_{m_0+M} = (m_0+M)\Delta + \tau_n$. Then the semblance coefficient is defined as follows,

$$S = \frac{\sum_{m=m_0}^{m_0+M} \left\{ \sum_{n=1}^{N} u_n(t_m + \tau_n) \right\}^2}{N \sum_{m=m_0}^{m_0+M} \sum_{n=1}^{N} u_n(t_m + \tau_n)^2} \tag{2}$$

The value of S depends on τ_n. When signals are coherent and τ_n is chosen to match the time lag of an actual wave field for each sensor, S takes the maximum. The value of τ_n is calculated for each sensor for a given parameter set (θ, s). When θ and s are in agreement with the true values, S should take the maximum.

The obtained semblance coefficients for different time windows usually show substantial scatters, suggesting the necessity of some sort of smoothing. We suppose that there are J time windows. After we calculate the semblance coefficients $S_j(\theta, s)$ for each of

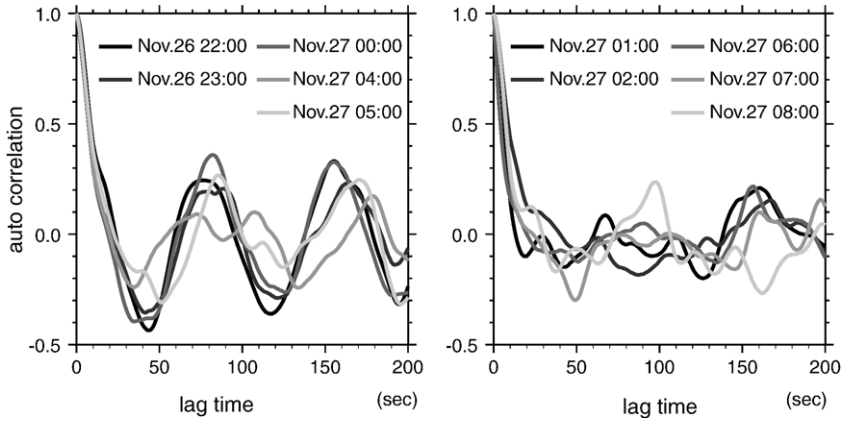

Fig. 4. Auto-correlation functions of the 10 s moving averages of the absolute value of the amplitudes observed on Nov. 26, 1999 at sensor 00 of the west array. We use the first 600 s of the data in every hour. The horizontal and vertical axes represent lag time (second) and auto-correlation coefficient, respectively. (Left) Examples for the time windows which show periodic amplitude modulations. Most of them show a peak at the lag time of about 80 s. (Right) Examples for the time windows which show aperiodic modulations. Although no periodic change in amplitude is clearly seen, the amplitudes do change with time.

these data windows ($j=1,2,...,J$), we estimate the parameters θ and s by averaging these semblance coefficient over the J windows.

$$\overline{S}(\theta,s)=\frac{1}{J}\sum_{j=1}^{J}S_j(\theta,s) \quad (3)$$

The parameter set (θ, s) for which the averaged semblance $\overline{S}(\theta,s)$ takes the maximum value is regarded as the most probable estimate of the parameter set. Based on our preliminary analysis, we set the searching range of azimuth and apparent slowness as −10° to 50° and 0.6 to 1.5 s/km for the west array, −80° to −50° and 0.4 to 1.0 for the north array. In this study azimuth is measured counterclockwise from east, so that azimuths 0° and 90° correspond to east and north, respectively. For the grid search, we use grid intervals of 0.02 s/km and 0.2° for apparent slowness and azimuth, respectively. In the actual analyses, we calculate semblance coefficients for 0.5 s time windows (called 'short window'). There is no overlapping between two adjacent short windows. We thus obtain 41 short windows from a record which is 20.5 s long. We call such a 20.5 s window as a 'long window'. For each long window we average the semblance coefficients for each parameter set over the 41 short windows in it. We then obtain one set of parameters, ($\hat{\theta}$, $\hat{s}$) which gives the maximum averaged semblance, $\overline{S}$, for the long window. The process is repeated for the next long window which is shifted by 1 s from the previous one. Finally we obtain a time series of the parameter set with 1 s intervals.

3.2. Estimation of epicentral region using two arrays

We can constrain the tremor epicenter reasonably well because of the presence of two arrays operated at the same time and because the arrival azimuths of the signal at the two arrays are well constrained. The details of the method to estimate the epicenter region are as follows; for each long time window we obtain two fan-shaped areas centered at the west and north arrays by taking the regions within the estimated error bounds of the azimuth deduced by the error estimation methods described below. We consider the area where the two fan-shaped areas overlap as the epicentral area. For example, for the data of 3000 s, 2980 of such the epicentral areas are obtained. Next, we divide the region around the main crater into grids of 10 m by 10 m. For each grid we count the number of long time windows whose epicentral areas include the grid. We regard the distribution of the number around the crater as representing the apparent epicentral area of the continuous tremor.

3.3. Synthetic tests for error assessment

3.3.1. Synthetic signals and noises

In this section, we use synthetic seismograms which consist of a tremor signal and two different types of noise in order to evaluate errors and biases in the tremor parameters. To generate a synthetic seismogram, we create random time series with a white spectrum and apply a band pass filter from 2.0 to 8.0 Hz, which corresponds to the dominant frequency band observed at the two arrays. The filtered signals are used for the synthetic tremor signals and the noises. Tremor signals propagate from a point source as spherical waves with the speed of 1.0 km/s and are recorded at the imaginary sensors which have the coordinates of the actual sensors (Fig. 1). We consider two types of noises, coherent noise and random noise. The coherent noise represents scattered waves which would originate from heterogeneous structure in the volcano edifice. In our synthetic test, they are considered to be plane waves arriving at the imaginary array from randomly sampled directions. The duration of each packet of the coherent noise is 0.5 s, and its velocity is the same as that of the tremor signal. The packets arrive at the array with the intervals which also are randomly sampled with the average of 0.5 s. On the other hand, the random noise is included to represent seismic noise associated with velocity structure beneath each seismometer. It has no coherency between any of the two imaginary sensors.

3.3.2. Evaluation of biases due to the plane wave assumption

The plane wave assumption causes a bias in our estimation of the azimuth θ. The closer the source is to the array, the larger is the azimuthal bias. From our preliminary analyses, the tremor sources could be regarded as at least 400 m distant from the west array, and 600 m from the north array. We evaluate the bias which depends both on the source azimuth and the distance using synthetic data without noise. For example, in the case of the west array, the estimated azimuth of a source which has the true azimuth of 20° ranges from 20° (for source distances of a few kilometers) to 24° (for distances of 400 m). In short, the azimuth for the west array tend to be overestimated by up to 4°. We calculate the range of bias for each source azimuth using the synthetic test, and expand

properly the estimated error ranges evaluated by the two methods mentioned below.

In addition to the plane wave assumption effect, the coherent noise affects the estimation of apparent slowness. Because of the presence of the coherent noise signals which arrive at the array from azimuths opposite to that of the tremor, the apparent slowness tends to be underestimated by up to 0.05 s/km. We expand the estimated error ranges for the apparent slowness evaluated by the two methods mentioned below.

3.3.3. Two methods of error assessment

We examine two methods for the evaluation of errors or uncertainties in the estimated parameters, θ and s. The first method is the one using threshold of semblance relative to the maximum semblance (Ohminato et al., 1998; Almendros and Chouet, 2003). As mentioned in Section 3.1, each long window contains 41 short windows, and we obtain the averaged semblance $\overline{S}(\theta,s)$ by averaging S_j over j for each pair of θ and s. We define $\hat{S}$ as the maximum value of $\overline{S}(\theta,s)$, and $P(0 \le P \le 1)$ as the threshold of relative semblance for defining the error range. We obtain the range of the parameter set (θ, s) for which $\overline{S}(\theta,s)$ takes a value exceeding $P \times \hat{S}$, and after the correction of the biases mentioned above define it as the error range. The parameter set ($\hat{\theta}$, $\hat{s}$) which gives $\hat{S}$ is regarded as the most probable parameter set.

The value of the threshold P is chosen based on a synthetic test as follows. In this test the tremor signals with amplitude of 1.0 (of an arbitrary unit) and a speed of 1.0 km/s are radiated from an imaginary surface source which is located at the center of the main crater. Synthetic seismograms are computed for imaginary seismic receivers at the locations of the actual sensors of the 1999 west array. We compute 12 sets of the seismograms. Six of the 12 sets contain random noise whose amplitude is either 0.2, 0.33, 0.5, 1.0, 2.0, or 3.0, but do not contain coherent noise. The other 6 sets contain no random noise but contain coherent noise with amplitude of either 0.2, 0.33, 0.5, 1.0, 2.0, or 3.0. The length of each seismogram is 1021 s. There are 1000 long windows for each seismogram, and each long window has overlapping of 19.5 s with the two adjacent windows. We estimate the parameters for the synthetic data, obtaining 1000 sets of parameters and error ranges for each of the 12 sets of the seismograms. For various values of the semblance threshold P, we calculate the percentages of the number of long windows for which the true parameters fall inside the error range. When we set P to 0.996, the true parameters fall within the error range for more than 69% (one sigma) of the time windows for all of the 12 sets of seismograms. We therefore choose 0.996 as the value of P.

The second method for error evaluation uses bootstrap (Efron and Tibshirani, 1993). There are 41 short windows (0.5 s long) in a long window (20.5 s long). For each short window included in the long window, we calculate the semblance coefficients, $S_j(\theta,s)$ ($j=1,2,\ldots,41$) for the given ranges of θ and s. We call the group of these 41 samples of semblance coefficients as a function of θ and s, as the original set of semblance, or simply as "the original set". We obtain an original set of semblance from a long window. Then we take a semblance $S_j(\theta,s)$ from the original set 41 times with replacement, and make another set named as a bootstrap resample set of semblance. Each bootstrap resample set therefore consists of 41 samples of S_j ($S_{j(l)}(\theta,s)$: $l=1,2,\ldots,41$: $j(l)$ is a number which is randomly picked up from a set of numbers {1, 2, 3,..., 41}). We repeat the procedure K times obtaining K bootstrap resample sets of semblance. The k-th resample set is represented as $S^k_{j(l)}(l=1,2,\ldots,41)$ ($k=1,2,\ldots,K$), where k represents the number of bootstrap resample. For each pair of θ and s, we average $S^k_{j(l)}$ over l as mentioned in Section 3.1, and estimate the most probable parameter set for the k-th bootstrap set, ($\hat{\theta}_k$, $\hat{s}_k$) ($k=1,2,3,\ldots,K$), for each long window. We set K to 50 in this study. For the two parameters, we calculate the averages ($\tilde{\theta}$, $\tilde{s}$) and the standard deviation (σ_θ, and σ_s) over k. We regard $\tilde{\theta}$ and $\tilde{s}$ as the estimates of the parameters, and $\tilde{\theta}+\sigma_\theta$ ($\tilde{\theta}-\sigma_\theta$) and $\tilde{s}+\sigma_s$ ($\tilde{s}-\sigma_s$) as the upper (lower) bounds of the error ranges. We perform the same synthetic test as for the first method, and confirm that the true parameters are within the error ranges for more than 69% (one sigma) of the long windows. Examples of the estimated parameters and error ranges estimated by the two methods are shown in Fig. 5. In this study we adopt the first method using the semblance threshold, because it gives more conservative estimates for the error ranges than the bootstrap method. The bounds of the error ranges of azimuth and apparent slowness are corrected for the biases.

4. Analysis of the 1999 data

4.1. Amplitude modulation and migration of epicenter

Figs. 6 and 7 show the results obtained from the data of the west array and the north array, respectively. The apparent azimuth and the amplitude of the epicenter of the continuous tremor clearly change with time. Their changes often synchronize quite well (second row of

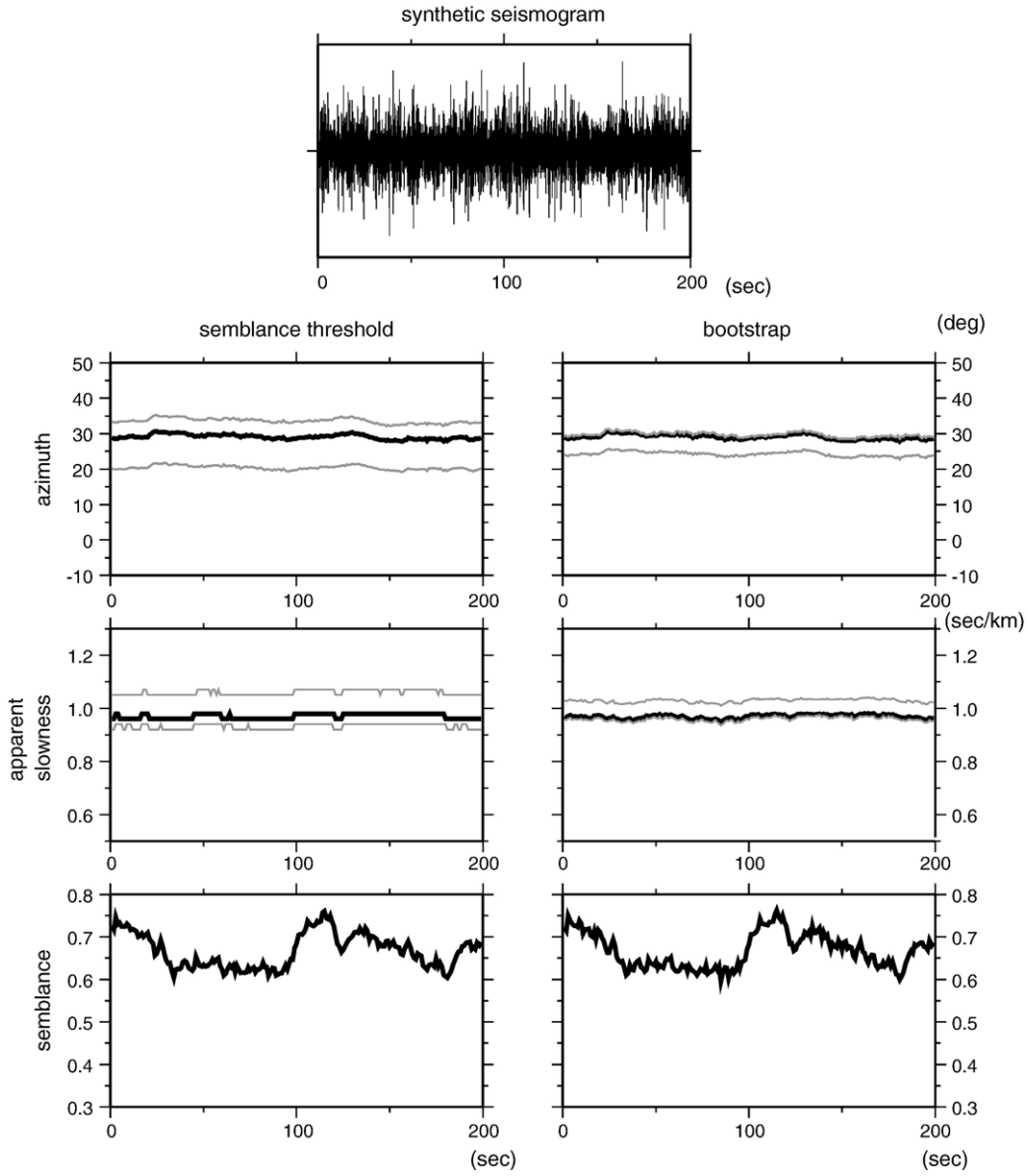

Fig. 5. Source parameters estimated from the synthetic seismograms for the 1999 west array. (Top) Synthetic vertical seismogram for a 200 s time window. (Second row) Azimuth of the epicenter from the center of the array measured counterclockwise from east. The azimuths of 0° and 90° correspond to east and north, respectively. Solid line shows the estimated parameters, and gray lines show the error ranges evaluated by the method using semblance threshold (left) and bootstrap (right). Because the estimated azimuth tends to be overestimated due to the plane wave assumption, the error ranges are asymmetric about the estimated values. (Third row) Apparent slowness in seconds per kilometer. Details are the same as the second row. Because the estimated slowness tends to be underestimated due to the coherent noise, the error ranges are asymmetric about the estimated values. (Bottom) Semblance coefficients. The true values of azimuth and apparent slowness are 27° and 1.0 s/km, respectively.

Fig. 6). This synchronization is more evident for the west array, but it is seen also for the north array (Fig. 7a). On the other hand, the apparent slowness and semblance values do not synchronize with the amplitudes as clearly as the azimuth (third and bottom rows of Figs. 6 and 7). As a result of the synchronization between the azimuth and amplitude, the apparent epicenter tends to be located southeastward when the amplitude is large, while it migrates northwestward when the amplitude is small (Fig. 6 second row), resulting in an epicentral area extending NW to SE. We plot the number of time windows described in details in Section 3.2 on the map with gray scale (Fig. 8). Another noticeable observation is

that the amplitude of the continuous tremor modulates sometimes periodically with a period of about 80 s (Fig. 4). Figs. 6a and 7a show the time windows which correspond to periodic modulation, while Figs. 6b and 7b are for aperiodic modulation.

There are two possibilities to explain the synchronization between the changes in tremor amplitude and epicentral azimuth. One is that the source of the tremor actually moves to-and-fro synchronized with the modulation in its amplitude. The other is that there are two or more tremor signals from different sources with fixed locations, and the amplitudes of the tremor signals modulate on some occasions with a period near 80 s but on the other occasions aperiodically. The estimated source parameters vary according to which of the tremor signals dominate on the seismograms. The latter model seems much more plausible, since in the former model the tremor sources must migrate more than 300 m within

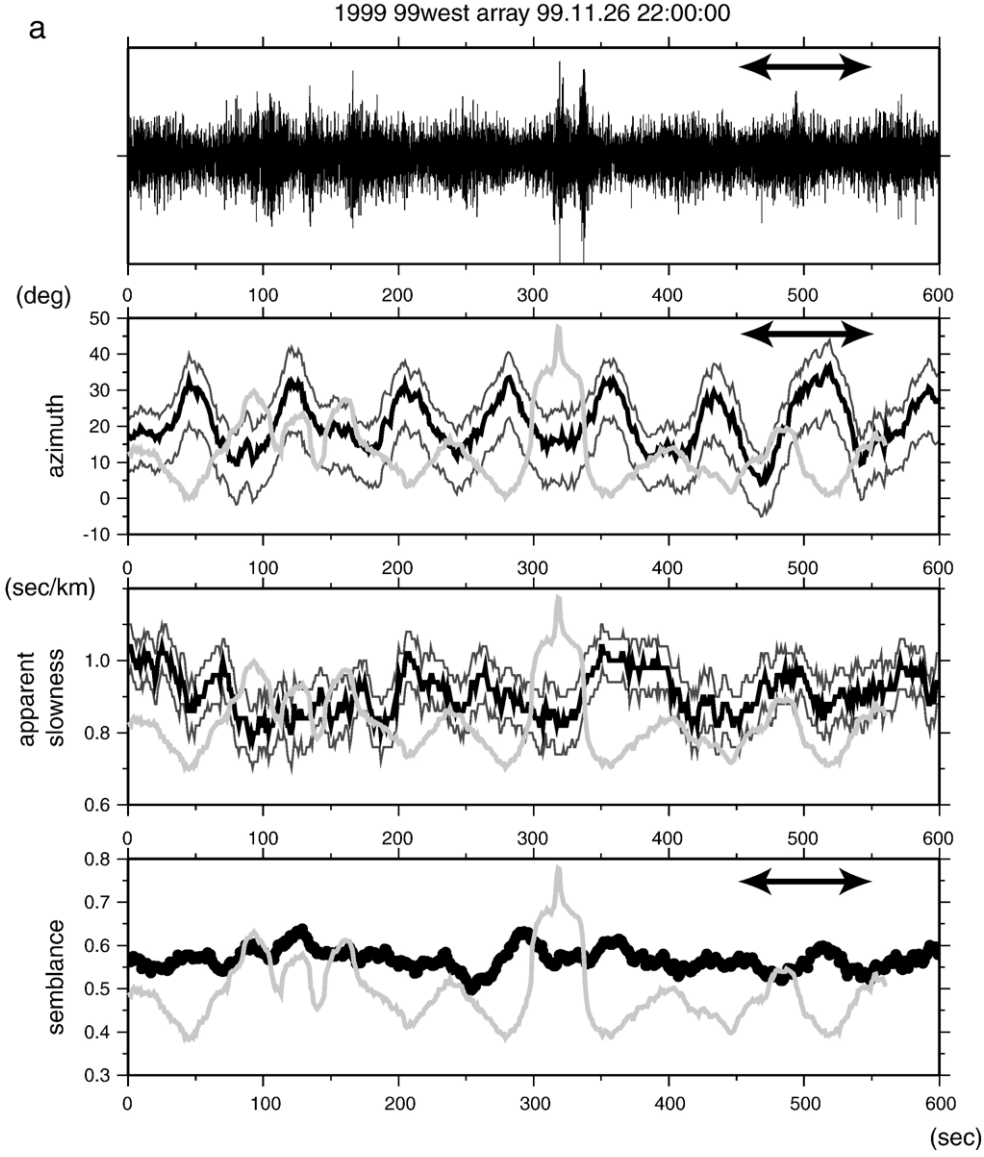

Fig. 6. Examples of the estimated parameters for the west array data plotted against time (in seconds). Examples for the time windows which show periodic amplitude modulation (a) and aperiodic modulation (b) are shown. Velocity seismogram of vertical component at station 00 (top), azimuth (in degree, measured counterclockwise from east) (second row), apparent slowness in seconds per kilometer (third row), and semblance coefficient (bottom row). The azimuth of the main crater is 2°. The estimated parameters are plotted by thick solid lines with error bounds (thin solid lines). In each panel, the RMS of the amplitude is superimposed with light gray line. The RMS amplitudes are calculated over a time windows of 20.5 s shifted by 1 s. The solid arrows correspond to the duration used to be matched with the synthetic data in Section 4.2.

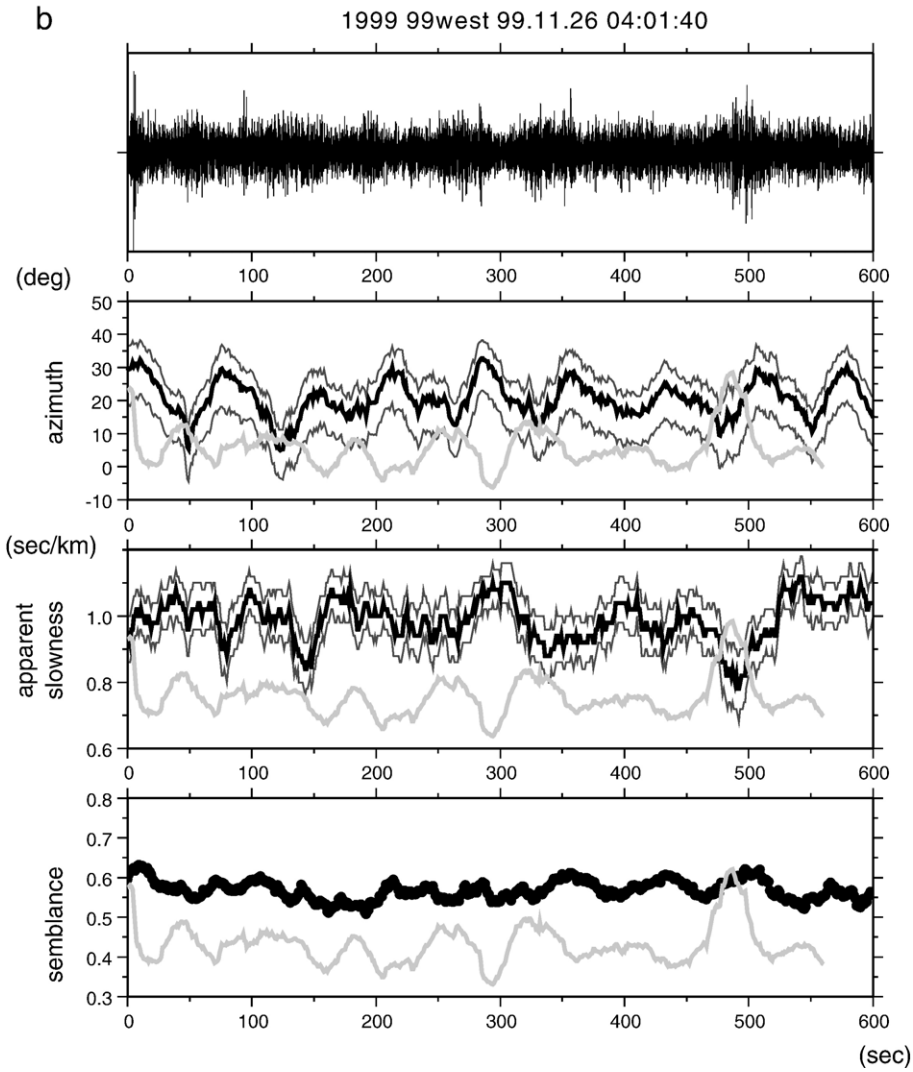

Fig. 6 (*continued*).

80 s when a periodic modulation occurs, requiring a migration speed more than 3 m/s. In this study we assume for simplicity that there are two sources and the signal amplitudes of only one of the sources modulate.

We note here that simple applications of semblance method, of f–k spectrum, or of MUSIC (Goldstein and Archuleta, 1987; Goldstein and Chouet, 1994; Chouet et al., 1997; Almendros et al., 2001; Saccorotti et al., 2004) to the modulated data, do not resolve two or more separated signals. This is confirmed by applying these methods to synthetic data which are computed for the models with two sources. We infer that the aperture of the 1999 west array is too small for resolving the two sources. The amplitude modulation does provide us with a chance to infer the presence of two or more sources, and we describe another method to estimate the two source locations in the next section.

4.2. Estimation of the two source locations

In this section we estimate the locations of the two sources by performing a synthetic data analysis. In the first step we analyze synthetic signals for two tremor sources with a variety of locations around the main crater, and locate "single source" epicenter, or "apparent epicenter" by assuming that there is only one tremor source as we did for the real data. The estimated apparent epicenter depends on the amplitude ratio between the two sources, and tends to be located between the two sources, on a line connecting the two

sources. In our analyses of the 1999 data, the apparent epicenters seem to be distributed along a line striking NW–SE. This suggests that the two sources are located on the line around which the apparent source regions are observed (Fig. 8). Fig. 9a shows the locations (called 0 to 10) of the two sources tested in the second step of the synthetic analysis. The depths of the imaginary sources are at the surface of the main crater lake. One of the two imaginary sources is called "NW source" considering that this is located northwest of the other source, and the other is called "SE source".

The apparent epicenters are affected by the two source locations and the amplitudes of the signals and noises. We test many patterns of the synthetic seismograms which have different source locations and different amplitudes of signals and noises, and examine how well the estimated parameters match the observations. For the synthetic data, we define A, B, and R as the RMS amplitudes of the tremor signals from the NW source, the tremor signals for the SE source, and the amplitudes of random noise, respectively. A and B satisfy the equations,

$$B = B_1 + B_2\left\{1 + \cos\left(-\pi + \frac{2\pi t}{T}\right)\right\} \qquad A + B_1 + B_2 = 10 \tag{4}$$

where T is the period of modulation, $T=80$ (s). The source locations of the NW and SE sources are

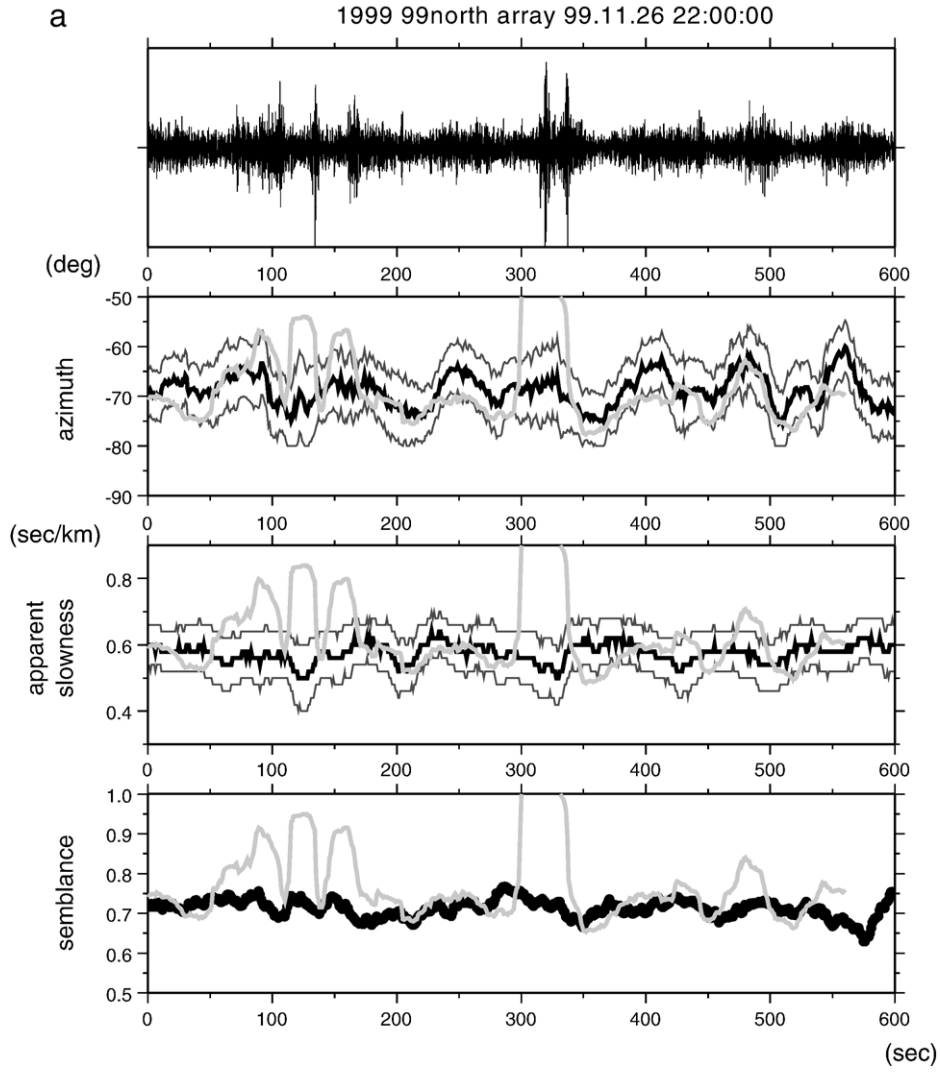

Fig. 7. The estimated location parameters for the 1999 north array for the same time windows as that of Fig. 6a and b. Note that azimuth measured counterclockwise from east is negative for this array, and the azimuth of the main crater is −63°. Other details are the same as those of Fig. 6.

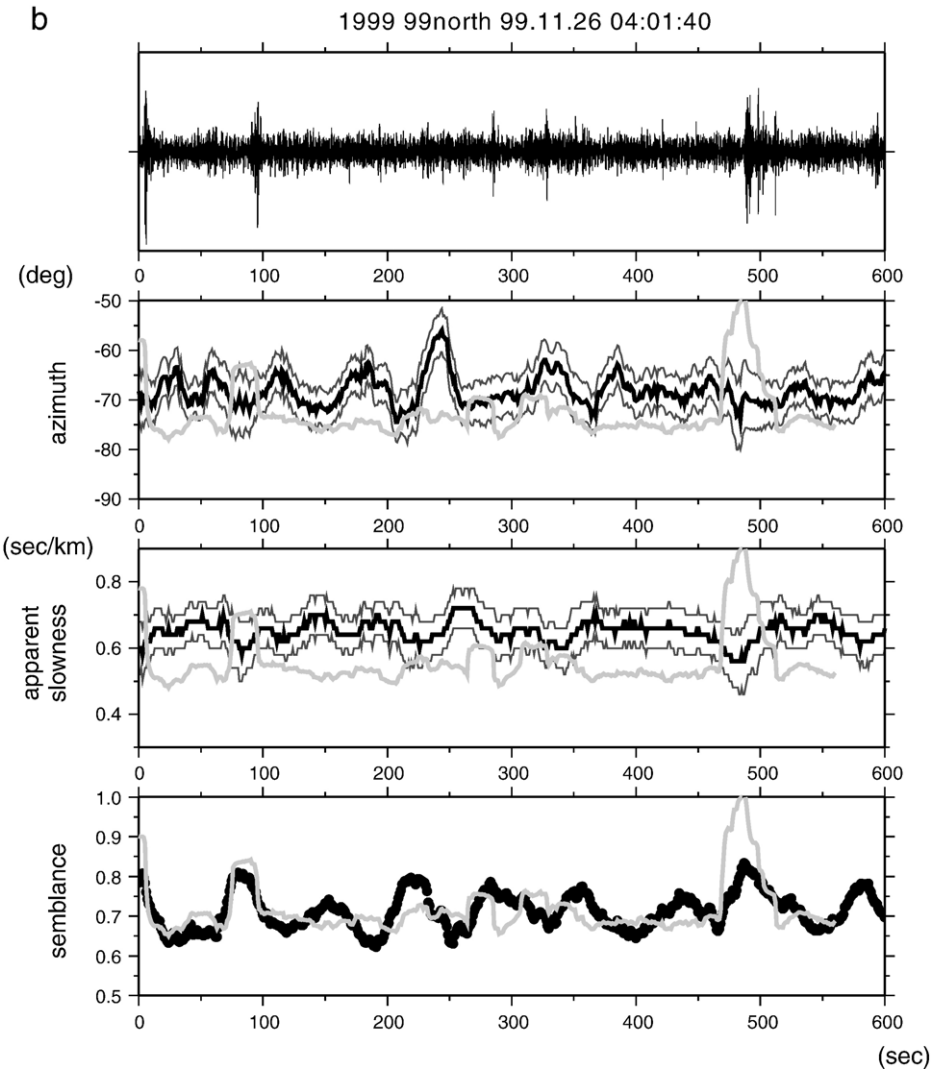

Fig. 7 (*continued*).

represented by the source number shown in Fig. 9a, and defined as L_{NW} and L_{SE}, respectively. In the following analysis, we neglect coherent noise for simplicity. We use the seismograms of the west array with duration of 100 s from 22:07:30 on Nov. 26 (Fig. 6a) as the observed data to be matched. The duration of each synthetic seismogram is 110 s. The maxima and minima of the parameters which are obtained by the averaged semblance method (Section 3.1) are computed for the observed seismograms ($\hat{\theta}^{max}_{obs}$, $\hat{\theta}^{min}_{obs}$, $\hat{a}^{max}_{obs}$, $\hat{a}^{min}_{obs}$) and for the synthetic seismogram ($\hat{\theta}^{max}_{syn}$, $\hat{\theta}^{min}_{syn}$, $\hat{a}^{max}_{syn}$ $\hat{a}^{min}_{syn}$). The model parameters are A, B_1, B_2, R, L_{NW}, and L_{SE}. The tested ranges of model parameters are shown in Table 1.

We introduce three penalty coefficients; azimuthal penalty coefficient p_θ, amplitude penalty coefficient p_a, and semblance penalty coefficient p_s. They are defined below to be small when the parameters estimated from the synthetic data and those from the observations are compatible. The azimuthal penalty coefficient p_θ is defined as,

$$p_\theta = w_\theta[|\hat{\theta}^{max}_{obs} - \hat{\theta}^{max}_{syn}| + |\hat{\theta}^{min}_{obs} - \hat{\theta}^{min}_{syn}| + \gamma_\theta] \quad (5)$$

where $\hat{\theta}^{max}_{obs}$ and $\hat{\theta}^{min}_{obs}$ are the maximum and minimum azimuths estimated from the observed seismograms described above, while $\hat{\theta}^{max}_{syn}$ and $\hat{\theta}^{min}_{syn}$ are the maximum and minimum azimuths for the synthetic seismograms. w_θ and γ_θ are constants which are introduced in order to

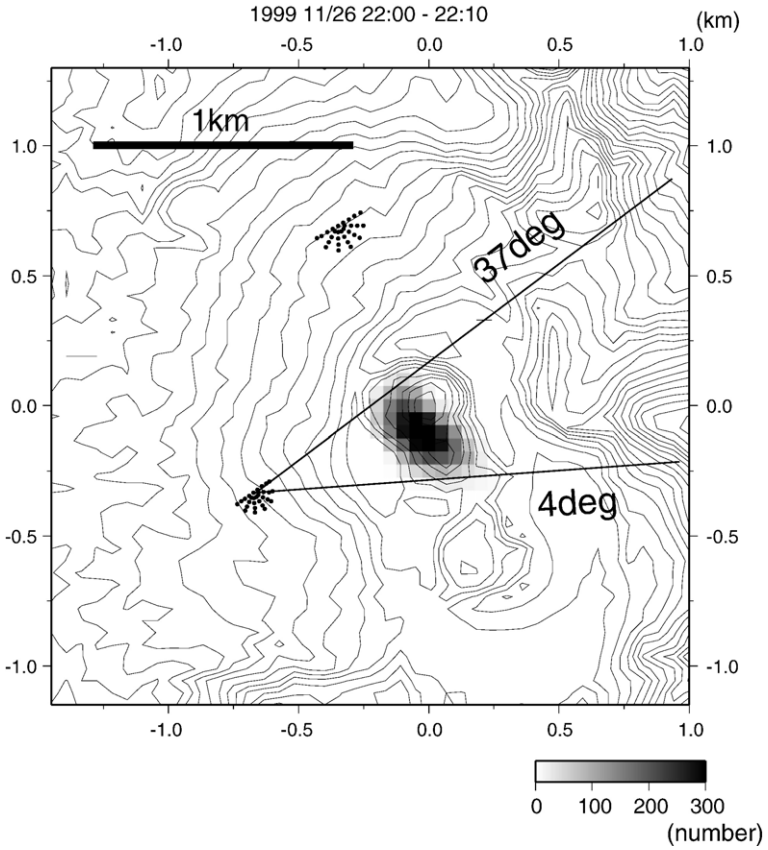

Fig. 8. An example of the area of apparent tremor epicenters for the west array data, estimated for 10 min starting from 22:00, November 26, 1999 (the same data as that of Figs. 6a and 7a). The number of long time windows whose source areas include each grid point is shown with gray scale. The epicentral area is seen as a smudge south of the crater. Two solid lines show the maximum and minimum values of estimated azimuth of the west array for the 10 min (See the second panel of Fig. 6a. Apparent azimuth takes maximum value of 37° at 519 s, and minimum value of 3° at 468 s).

normalize the minimum and maximum values of p_θ from 0 to 1, respectively. Because the estimated azimuths are not much affected by the noise amplitude R, we fix R to 0, so that p_θ is a function of L_{NW}, L_{SE}, A, B_1, and B_2. In a similar way, the amplitude penalty coefficient is defined as,

$$p_a = w_a[|a_{obs}^{max} - a_{syn}^{max}| + |a_{obs}^{min} - a_{syn}^{min}| + \gamma_a] \quad (6)$$

where a_{obs}^{max} and a_{obs}^{min} represent the maximum and minimum RMS amplitudes of the observed seismograms of the center of the west array, while a_{syn}^{max} and a_{syn}^{min} are those for the synthetic seismograms. w_a and γ_a are constants to normalize p_a from 0 to 1. A similar penalty coefficient is defined also for semblance as,

$$p_s = w_s[|\langle \hat{S} \rangle_{obs} - \langle \hat{S} \rangle_{syn}| + \gamma_s] \quad (7)$$

where $\langle \hat{S} \rangle$ is the averaged $\hat{S}$ over the entire data window. w_s and γ_s represent constants which we introduce to normalize the minimum and maximum value of p_s from 0 to 1. We calculate p_a and p_s fixing $L_{NW}=4$ and $L_{SE}=3$, anticipating that they do not depend much on the source locations, so that these two coefficients are functions of A, B_1, B_2, and R. We then obtain the penalty coefficient p by summing up these three coefficients as,

$$\begin{aligned} p(L_{NE}, L_{SE}, A, B_1, B_2, R) &= p_\theta(L_{NE}, L_{SE}, A, B_1, B_2) + p_a(A, B_1, B_2, R) \\ &\quad + p_s(A, B_1, B_2, R) \end{aligned} \quad (8)$$

Finally, for each pair of the source locations (L_{NW}, L_{SE}), we search the parameters of A, B_1, B_2, and R for which p takes the minimum value for the ranges shown in the Table 1. Fig. 9b shows the minimum penalty coefficient as a function of L_{SE} with L_{NW} as a parameter. Each line in the figure corresponds to a different L_{NW}. The minimum p corresponding to the best fit to the observations is obtained for $L_{NW}=7$ and $L_{SE}=1$. For this pair the estimated amplitudes are $A=4$, $B_1=2$,

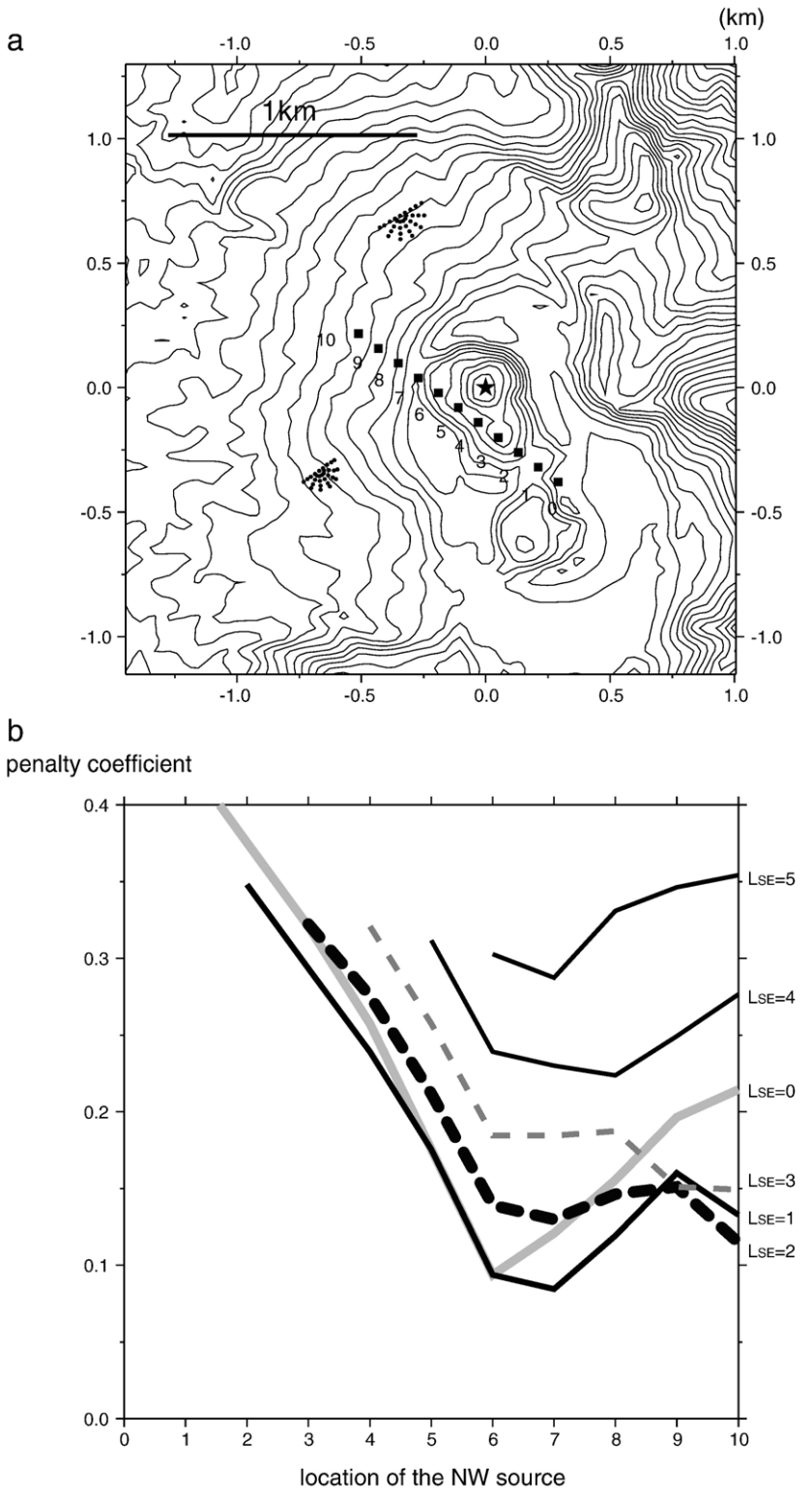

Fig. 9. (a) Locations of the imaginary sources used for the synthetic test to determine the two source locations. In the test, the source locations of the NW and SE sources are represented by the source number shown in this figure, and defined as L_{NW} and L_{SE}, respectively. (b) The minimum penalty coefficient as a function of L_{NW} with L_{SE} as a parameter. Different lines correspond to the minimum penalty coefficients for different L_{SE}. The penalty coefficients take small values when we choose L_{SE} smaller than 3, and L_{NW} larger than 6. When we set L_{SE} to 1, the penalty coefficient takes a minimum value for $L_{NW}=7$.

Table 1
The ranges of the model parameters of the synthetic test

L_{SE}	0, 1, 2, 3, 4, 5
L_{NW}	$L_{SE}+1$, $L_{SE}+2$,.., 10
A	1, 2, 3, 4, 5, 6, 7, 8, 9
B_1	0, 1,.., 9–A, 10–A
B_2	10–A–B_1
R	0, 1,.., 19, 20

$B_2=4$, and $R=6$. Figs. 10 and 11 show the parameters at the west array and the apparent epicentral area determined from the synthetic data, respectively. When we choose L_{NW} slightly different from 7, L_{SE} tends to be less than 2. Although the source locations and amplitudes somewhat depend on the observation time window used making their estimates somewhat uncertainties, the SE source tends to be located more than 400 m distant from the NW source. We therefore conclude that the two sources are separated by more than 400 m although the absolute locations of the two sources are less certain.

5. Discussion

5.1. Comparison with the tremor source for the 2001 observation

About two years after the 1999 experiment, we installed a larger cross-shaped array near the main crater

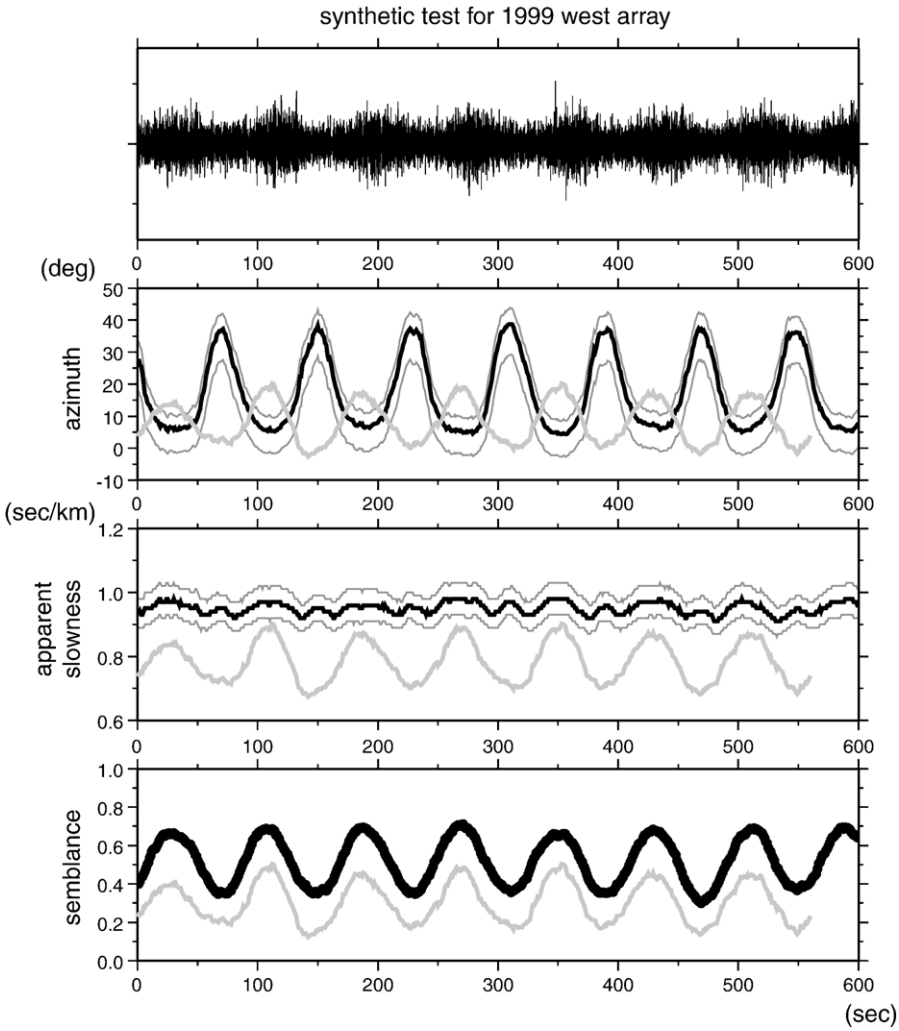

Fig. 10. Estimated parameters for the synthetic data at the west array. Synthetic parameters are chosen to make the penalty coefficient minimum ($L_{NW}=7$, $L_{SE}=1$, $A=4$, $B_1=2$, $B_2=4$, $R=6$). Seismogram at station 00 (top), azimuth (second row), apparent slowness in seconds per kilometer (third row), and semblance coefficient (bottom row) are shown. The estimated parameters are plotted by solid lines with error bounds. In each panel, the RMS of the amplitude is superimposed with a line of light gray.

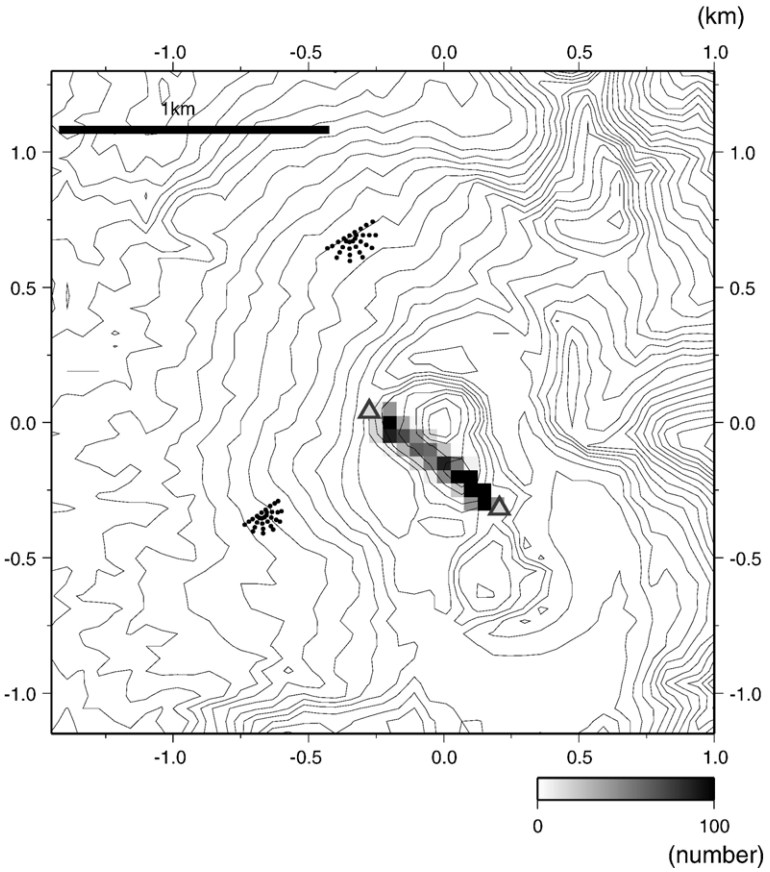

Fig. 11. Apparent epicentral area determined from the synthetic data. Seismograms used are the same as that in Fig. 10. Two imaginary sources ($L_{NW}=7$, $L_{SE}=1$) are marked by triangles.

in July, 2001 (Fig. 1). Fig. 12 shows the results obtained from the 2001 array data. Since this array has a much larger aperture, we could locate the tremor epicenter by using only one array on the basis of an assumption of cylindrical wave radiation from epicenters. The azimuth of the epicenter is estimated to be about 35–45° counterclockwise from east, and the epicentral distance is around 400 m. The estimated apparent slowness is in the range of 0.7–1.0 (s/km). We should mention that at the time of the 2001 observation, the activity of the SE source whose amplitudes modulated in 1999 has been decayed. On the other hand the northwest source of the 1999 data may be identical to the tremor source of the 2001 data. This may infer that the NW source has a sustained supply of heat or volcanic gas from below, while the supply to the SE source ceased sometime after the 1999 experiment. The stability of the heat or gas supply to a shallow tremor source from depth would depend on the state of conduits through which volcanic gas flows. Although our observations might have caught a change in the conduit state below the main crater at Aso, we do not have enough information to discuss extensively what controls temporal change in the supply of volcanic gas at this stage.

5.2. The extent and the depth of the tremor source

We note here that a real tremor source should have a finite extent, and the epicenters we have located may be regarded as the centroid location of the seismic moment release. The real extent of each tremor source is difficult to estimate accurately. For example, although the epicentral area estimated for the 2001 data forms a narrow band-like area (Fig. 12), it may not necessarily mean that the source region actually is as such.

We cannot estimate the source depth directly from the estimated values of the apparent slowness because the observed signals could contain surface waves and body waves. Mori (2000) showed that the earliest part of the isolated events (Type c) seismograms mostly consists of body waves whose apparent slowness is about 0.2 s/km. They also determined the source depth

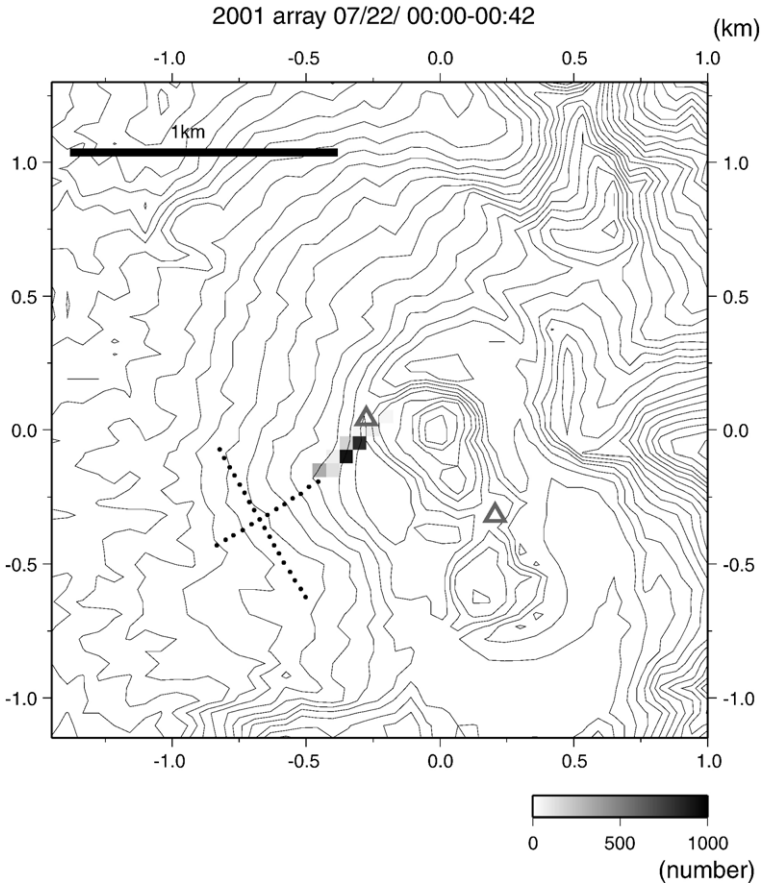

Fig. 12. An example of the area of the apparent tremor epicenters for the 2001 array data, estimated for 43 min from 22:00:00 on Jul. 22, 2001. The number of long time windows whose source areas include each grid point is shown with gray scale. The sensor locations for the 2001 observation are also plotted. Triangles show the locations of two imaginary point sources estimated for the 1999 data (see text).

of the isolated events at about 600 m. The apparent slowness values of the continuous tremor are much larger than that of the isolated events, so that we may safely infer that the source depth of the continuous tremor is shallower than 600 m.

5.3. Cause of the amplitude modulation

The mechanism of the amplitude modulation is not necessarily clear at this stage. Ohminato and Davide (1997) observed modulation of tremor amplitude at Satsuma-ioujima. The period of the modulation they report is 50 min, which is much longer than that of Aso. They infer that the continuous tremor is generated at a vent which emits volcanic gas, and that the modulation reflects the fluctuation in the gas emission rate that is caused by the convection of magma in the conduit. At Aso, juvenile magma seemed not to exist at the shallowest part of the volcano edifice during the period of the two experiments, and no obvious changes concomitant with the modulation was observed for the fumarole activity, so that any mechanism associated with periodic magma convection is unlikely. Hydrothermal processes are more plausible for the mechanism than magma processes.

Hydrothermal origin of volcanic tremor is also suggested for at Kilauea volcano by Almendros et al. (2001), although they do not report any modulation of tremor amplitude. They determine the source region of tremor at 200 m northeast of the Halemaumau pit crater. The tremor source has a size of about $0.6 \times 1.0 \times 0.5$ km and its depth is shallower than 200 m. There is a gap between the location of the epicenter region and the center of the crater, as is in the case of Aso.

An alternative idea of the cause of the modulation would be the mechanism which drives a geyser. Kieffer (1984) points out the relations between the seismicity and the eruption cycle of Old Faithful Geyser in Yellowstone National Park. A cycle of the geyser is as follows: (1) an underground reservoir is filled with

water, (2) the temperature of the water rises and reaches to the boiling point, (3) the water/steam mixture is emitted out of the conduit until the reservoir is empty. According to this model, the interval of the eruptions depends on the size of the reservoir, water flow rate into the reservoir, and the rate of the heat transfer. The interval of the cycle of the Old Faithful Geyser is a few tens of minutes, which is again much longer than that of Aso (80 s).

The geyser model needs a large amount of the liquid water which is enough to fill the hot reservoir. For the Aso volcano the existence of a large amount of ground water under the active crater has been suggested by previous researchers. Hase et al., (2005) detected low resistivity regions at the depths of about 200 m and about 1000 m under the active crater by the Magneto-Telluric (MT) observations. Tanaka (1993) proposes the occurrence of rapid heating/cooling about 200 m below the active crater lake during the 1989 eruptive activity based on the observations of the temporal change in the local magnetic dipole, and attributes it to the interaction of groundwater and superheated vapor. These seem to support a geyser-type model for the mechanism of the amplitude modulation at Aso, but details of the model, especially regarding the mechanism of rapid discharge of water from the underground reservoir, remain unclear.

Yamamoto et al. (1999) detected a crack-like conduit at a few hundred meters southwest of the active crater at Aso. The best estimate of the upper edge of the crack is at the depth of 400 m below the crater lake. The continuous tremor is possibly generated near the transport paths of the volcanic gas and/or magma which connect the upper edge of the crack-like conduit and the conical-shaped vent just below the active crater. The source region of the continuous tremor may thus reflect the structure of the conduit system at the uppermost edifice of the Aso volcano.

6. Conclusions

We analyze the seismic array records of the continuous tremor observed in 1999 at Aso volcano, and accurately locate the epicenters of the tremor. The estimated azimuth of the epicenter often changes with time being synchronized with the tremor amplitude. If we assume the presence of two point sources with fixed locations, one of them is located at 300 m west of the center of the active crater (NW source) and the other at 200 m south of the crater (SE source). The estimated location of the NW source in 1999 is close to that in 2001, possibly being identical. The cause of the amplitude modulation might be explained by a geyser-type mechanism. The source region of the continuous tremor may represent the structure of the conduit system at the uppermost part of the Aso volcano.

Acknowledgements

We would like to thank all who participated in the observations: M. Sako, T. Hashimoto, M. Nakabou, M. Kato, T. Ohminato, J. Oikawa, G. Helffrich, A. Okabe, T. Nakajima, and K. Iwamura. We could not complete this work without their help. Comments by the two anonymous reviewers greatly improved this paper. We are indebted to Y. Tanaka, H. Hase, and M. Utsugi (Aso Volcanological Laboratory) for valuable discussion. We thank T. Tsutsui for his advice about the velocity structure of the Aso volcano.

References

Almendros, J., Chouet, B., 2003. Performance of the radial semblance method for the location of very long period volcanic signals. BSSA 93, 1890–1903.

Almendros, J., Ibanez, J.M., Alguacil, G., Del Pezzo, E., 1999. Array analysis using circular-wave-front geometry: an application to locate the nearby seismo-volcanic source. Geophys. J. Int. 136, 159–170.

Almendros, J., Chouet, B., Dawson, P., 2001. Spatial extent of a hydrothermal system at Kilauea Volcano, Hawaii, determined from array analysis of shallow long-period seismicity. J. Geophys. Res. 106, 13565–13580.

Chouet, B.A., 1996. Long-period volcano seismicity: its source and use in eruption forecasting. Nature 380, 309–316.

Chouet, B., Saccorotti, G., Martini, M., Dawson, P., De Luca, G., Milana, G., Scarpa, R., 1997. Source and path effects in the wave fields of tremor and explosions at Stromboli Volcano, Italy. J. Geophys. Res. 102, 15129–15150.

Efron, B., Tibshirani, R.J., 1993. An Introduction to the Bootstrap. Chapman and Hall, New York.

Goldstein, P., Archuleta, R.J., 1987. Array analysis of seismic signals. Geophys. Res. Lett. 14, 13–16.

Goldstein, P., Chouet, B., 1994. Array measurements and modeling of sources of shallow volcanic tremor at Kilauea Volcano, Hawaii. J. Geophys. Res. 99, 2637–2652.

Hase, H., Hashimoto, T., Sakanaka, S., Kanda, W., Tanaka, Y., 2005. Hydrothermal system beneath Aso volcano as inferred from self-potential mapping and resistivity structure. J. Volcanol. Geotherm. Res. 143, 259–277.

Ibanez, J.M., Del Pezzo, E., Almendros, J., La Rocca, M., Alguacil, G., Ortiz, R., Garcia, A., 2000. Seismo volcanic signals at Deception Island volcano, Antarctica: wave field analysis and source modeling. J. Geophys. Res. 105, 13905–13931.

Ito, A., 1985. High resolution relative hypocenters of similar earthquakes by cross spectral analysis method. J. Phys. Earth 33, 279–294.

Kaneshima, S., Kawakatsu, H., Matsubayashi, H., Sudo, Y., Tsutsui, T., Ohminato, T., Ito, H., Uhira, K., Yamasato, H., Oikawa, J.,

Takeo, M., Iidaka, T., 1996. Mechanism of phreatic eruptions at Aso volcano inferred from near-field broadband seismic observations. Science 273, 642–645.

Kawakatsu, H., Kaneshima, S., Ohminato, T., Sudo, Y., Tutui, T., Uhira, K., Yamasato, H., Ito, H., Legrand, D., 2000. Aso seismic observation with broadband instruments. J. Volcanol. Geotherm. Res. 101, 129–154.

Kieffer, S.W., 1984. Seismicity at Old Faithful geyser: an isolated source of geothermal noise and possible analogue of volcanic seismicity. J. Volcanol. Geotherm. Res. 22, 59–95.

Kikuchi, S., 1963. On the short period volcanic micro-tremors at Mt. Aso. Bull. Volcanol. Soc. Japan 2, 9–16.

Lacoss, R.T., Kelly, E.J., Toksoz, M.N., 1969. Estimation of seismic noise structure using arrays. Geophysics 34, 21–38.

Legrand, D., Kaneshima, S., Kawakatsu, H., 2000. Moment tensor analysis of near field broadband waveforms observed at Aso volcano. J. Volcanol. Geotherm. Res. 101, 155–169.

Mori, T., 2000. Focal mechanism of short period volcanic tremor (HB-Tremor) during a calm period of Aso Volcano, Ph.D. Thesis, Kyoto Univercity.

Neidel, N.S., Taner, M.T., 1971. Semblance and other coherency measures for multichannel data. Geopysics 36, 482–497.

Neuberg, J., Luckett, R., Baptie, B., Olsen, K., 2000. Models of tremor and low-frequency earthquake swarms on Montserrat. J. Volcanol. Geotherm. Res. 101, 83–104.

Ohminato, T., Davide, E., 1997. Broadband seismic observations at Satsuma-Iwojima volcano, Japan. Geophys. Res. Lett. 24, 2845–2848.

Ohminato, T., Chouet, B., Dawson, P., Kedar, S., 1998. Waveform inversion of very long period impulsive signals associated with magmatic injection beneath Kilauea Volcano, Hawaii. J. Geophys. Res. 103, 23839–23862.

Saccorotti, G., Zuccarello, L., Del Pezzo, E., Ibanez, J., Gresta, S., 2004. Quantitative analysis of the tremor wavefield at Etna Volcano, Italy. J. Volcanol. Geotherm. Res. 136, 223–245.

Sassa, K., 1935. Volcanic micro-tremors and eruption-earthquakes (Part 1 of the geophysical studies on the volcano Aso). Mem. Coll. Sci., Univ. Kyoto, Ser. A 18, 255–293.

Takagi, N., 2002. Location of Tremor Sources at Aso Volcano Using Short Period Seismic Array Master Thesis, Tokyo Institute of Technology.

Tanaka, Y., 1993. Eruption mechanism as inferred from geomagnetic changes with special attention to the 1989–1990 activity of Aso Volcano. J. Volcanol. Geotherm. Res. 56, 319–338.

Yamamoto, M., 2004. Volcanic uid system inferred from broadband seismic signals Ph.D. Thesis, Tokyo Univercity.

Yamamoto, M., Kawakatsu, H., Kaneshima, S., Mori, T., Tsutsui, T., Sudo, Y., Morita, Y., 1999. Detection of a crack-like conduit beneath the active crater at Aso volcano, Japan. Geophys. Res. Lett. 26, 3677–3680.